FOSSEE, IIT Bombay
OpenFOAM Research Migration Project
April 22, 2022

# Forced convection past a semi-circular cylinder at incidence with a downstream circular cylinder

Saptarshi Joshi
*Department of Mechanical Engineering, IIT Bombay*

## Synopsis

This research migration project aims to do numerical simulations of forced convection past a semi-circular cylinder at incidence with a downstream circular cylinder [1] using `OpenFOAM`. The geometry and mesh were defined using ANSYS. The transient simulations were performed using the SIMPLE and PISO algorithms-based `pimpleFoam` solver. The thermo-fluidic transport is studied in the Laminar flow regime at a Reynolds number of $Re = 100$. The analysis executed by Sarkar et. al. [1] using commercial CFD code `Fluent` was taken as a reference for validation.

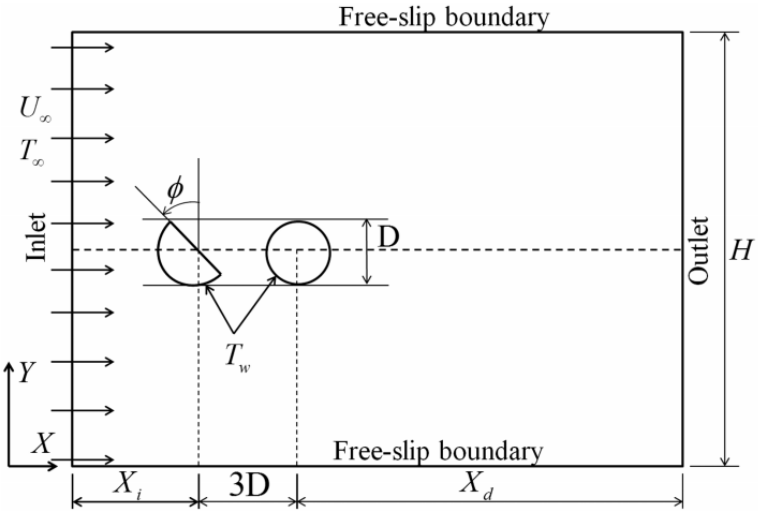


The angle of incidence of the semi-circular cylinder is $\phi = 45°$. The upstream, downstream distances and the height of the domain are chosen to be $X_i = 8D$, $X_d = 37D$ and $H = 20D$. Here, $D$ is the the projected diameter of the semi-circular cylinder and the diameter of the tandem circular cylinder.

# 1 Introduction

The reference [1] uses air, a Newtonian fluid, for the unsteady computations performed for a range of incidence angles $(\phi)$ and Reynolds number $(Re)$. The incidence angles are in the range $0° \leq \phi \leq 90°$ and the laminar flow is modeled in the Reynolds number range of $60 \leq Re \leq 160$. The numerical model generated using commercial CFD code `Fluent` was validated with the available experimental and numerical data from the literature for forced convection over a circular cylinder. The effect of these variations was studied using the engineering quantities; Coefficient of Lift $(C_{L,rms})$, Coefficient of Drag $(C_{D,rms})$, Nusselt number $(Nu)$ and Strouhal number $(St)$. Three vortex shedding regimes were identified by studying the streamlines, vorticity and temperature contours. The heat transfer characteristics were examined through average and local variations of Nusselt number over the cylinder walls. A global stability analysis through the dynamic mode decomposition also showed a stabilizing flow situation for the present range of operating parameters.

# 2 Governing Equations and Models

To reproduce results generated by Sarkar et. al. [1], `OpenFOAM-7` software was used. The Navier-Stokes equations for incompressible single-phase flows govern the fluidic transport along with the energy equation for thermal transport. The governing continuity, momentum and energy equations are given by:

$$\nabla \cdot \boldsymbol{u} = 0$$

$$\frac{\partial \boldsymbol{u}}{\partial t} + (\boldsymbol{u} \cdot \nabla)\boldsymbol{u} = \nu \nabla^2 \boldsymbol{u} - \frac{1}{\rho}\nabla p$$

$$\frac{\partial T}{\partial t} + (\boldsymbol{u} \cdot \nabla)T = \alpha \nabla^2 T$$

The above energy equation governs the thermal transport for incompressible subsonic flows. The laminar flow simulation requires no turbulence modeling.

# 3 Simulation Procedure

## 3.1 Geometry and Mesh

The geometry and mesh is created using the commercial code `ANSYS Meshing`.

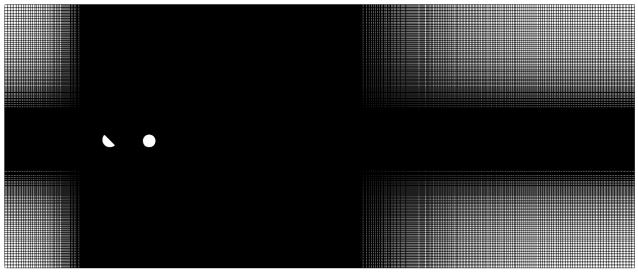

A 2-D structured mesh with hexahedral cells is generated. The total number of cells in the mesh are 278904. Nine meshing zones with different grading/biases are created such that the regions away from primary flow region have coarser mesh. A bias factor $(bf)$ of 7 and a growth rate $(r)$ equal to 1.2 is used. For an edge length $L$, length of first element $l$ and the number of divisions $n$, the grading in meshing can be mathematically represented by the following equations.

$$bf = r^{n-1}$$

$$L = \sum_{i=0}^{n-1} l * r^i$$

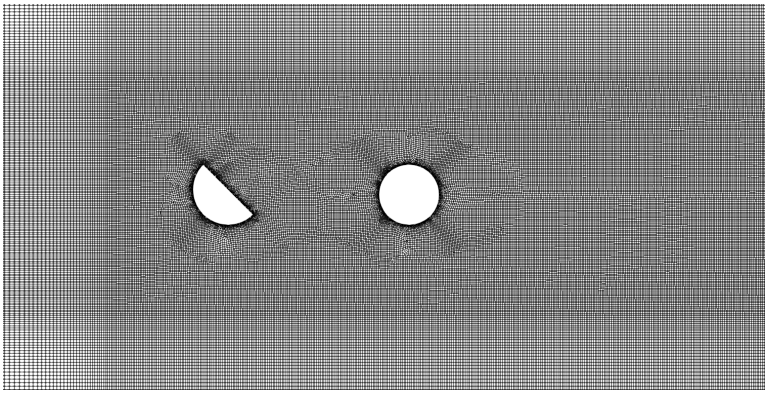

The central meshing zone surrounding the cylinders has an element size of 0.03 m. An unstructured mesh around the cylinders arises due to the geometry and refinement.

## 3.2 Initial and Boundary Conditions

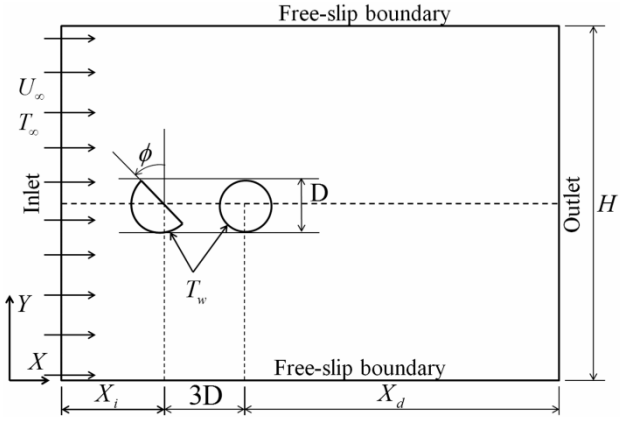


The inlet is a `fixedValue` uniform free-stream velocity $(u_\infty)$ inlet such that the Reynolds number $(Re)$ for the flow over the cylinders is 100 and the free-stream temperature $(T_\infty)$ to be 300 K. The cylinder walls are maintained at a constant wall temperature $(T_w)$ of 360 K. The cylinder walls have a `noSlip` boundary condition for the velocity. The top and bottom walls free-slip boundaries of the type `zeroGradient` for $p, u$, and $T$. The flow exits the domain through a zero gauge pressure outlet with `zeroGradient` for $u$ and $T$. The domain is initialized with zero velocities, pressures and a temperature of 300 K.

## 3.3 Solver

The flow simulation is conducted using the transient, incompressible solver `pimpleFoam`. The solution algorithm of `pimpleFoam` is derived from the algorithms SIMPLE and PISO.
To model thermal transport in forced convection, the energy equation for incompressible, subsonic flows needs to be solved. Thus, the solver is modified to incorporate the energy equation in its solution algorithm which resulted in the solver, `thermalPimpleFoam`. The energy equation is included in a new file `"TEqn.H"`. The equation is coded as

```
fvScalarMatrix TEqn
(
  fvm::ddt(T)
+ fvm::div(phi, T)
==
  fvm::laplacian(alphaTh, T)
);

TEqn.relax();
TEqn.solve();
```

The total time for simulation is 30100 s and the time step $\Delta t$ is 5 s. This time step is chosen to ensure that the Courant number $C = \frac{u\Delta t}{\Delta x}$ is less than 0.7 in the domain throughout the simulation.

For calculation of heat flux from the cylinder walls in post-processing, another solver `wallHeatFluxIncompressible` is used. The solver `wallHeatFlux` available in OpenFOAM can only be used with compressible solvers. As `pimpleFoam` is an incompressible solver, the modified utility `wallHeatFluxIncompressible` developed by Himanshu Sharma is used. The solver was further modified to match the OpenFOAM version 7 requirements and to suit laminar flow modeling.

# 4 Results and Discussions

The table below compares the results obtained using the present numerical model, the reference being used for research migration and the absolute percentage error in the calculated quantities. The Coefficient of Lift $(C_{L,rms})$, Coefficient of Drag $(C_{D,rms})$ and Nusselt number $(Nu)$ are tabulated for both semi-circular cylinder and the circular cylinder and the Strouhal number $(St)$ is separately calculated. Streamlines, Temperature and Voriticity contours are also plotted. A detailed analysis of the results has been presented in the following sections.

| | Semi-Circular Cylinder | | | Circular Cylinder | | | St |
|---|---|---|---|---|---|---|---|
| | Cd_RMS | Cl_RMS | Nu | Cd_RMS | Cl_RMS | Nu | |
| Literature | 1.600 | 0.367 | 4.975 | 0.411 | 0.779 | 3.883 | 0.126 |
| Present Numerical Model | 1.443 | 0.370 | 5.282 | 0.576 | 0.907 | 3.961 | 0.084 |
| Error (%) | 9.804 | 0.831 | 6.180 | 40.065 | 16.365 | 2.020 | 33.179 |

## 4.1 Force Coefficients

The force coefficients, Coefficient of Lift $(C_{L,rms})$ and Coefficient of Drag $(C_{D,rms})$ are calculated using the pressure and stresses acting on the cylinder walls.

$$C_D = 2\int_A (-pn_x + \tau_{xx}n_x + \tau_{xy}n_y)dA$$

$$C_L = 2\int_A (-pn_y + \tau_{xy}n_x + \tau_{yy}n_y)dA$$

where the non-dimensional stress components are given by

$$\tau_{ij} = \frac{1}{Re}\left(\frac{\partial u_i}{\partial x_j} + \frac{\partial u_j}{\partial x_i}\right)$$

For the semi-circular cylinder, the root mean squared (RMS) values for drag coefficient $C_{D,rms}$ has a variation of $10\%$ approximately, whereas, the lift coefficient $C_{L,rms}$ matches almost perfectly with the literature at a percentage deviation of $0.831\%$. Thus, the force coefficients are reasonably validated for the semi-circular cylinder, however, is not the case for the circular cylinder. The $C_{D,rms}$ and $C_{L,rms}$ for the circular cylinder have deviations as high as $\sim$ $40\%$ and $\sim$ $16\%$ respectively.

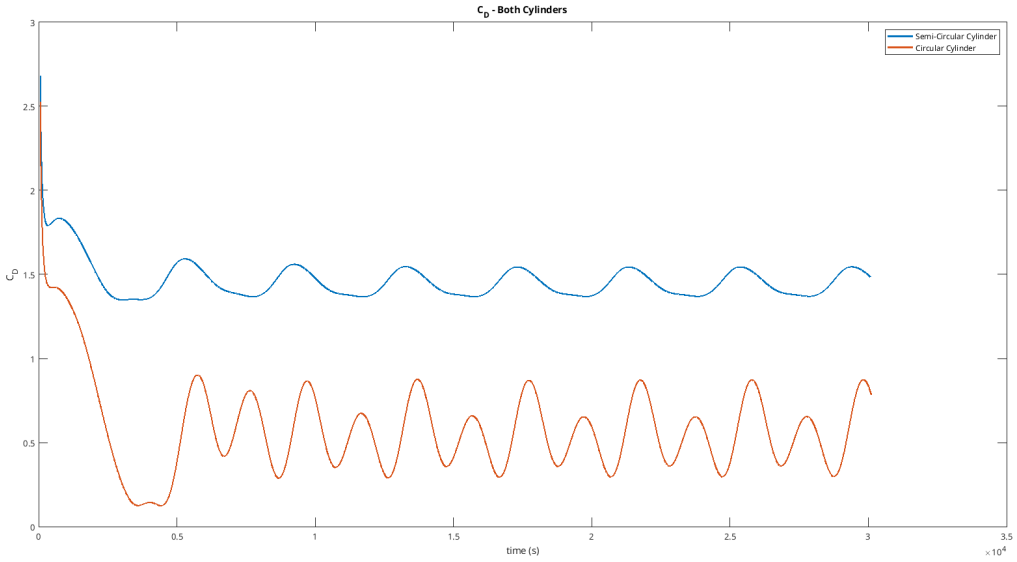


The plot above shows the variation of $C_{D,rms}$ with time for both the cylinders. The drag coefficient for the semicircular cylinder is higher, which is expected as the flow is incident directly on it creating higher pressure regions. The $C_{D,rms}$ initially drops and then forms repeating sinusoidal signals. This indicates that the dynamic steady state has been reached.

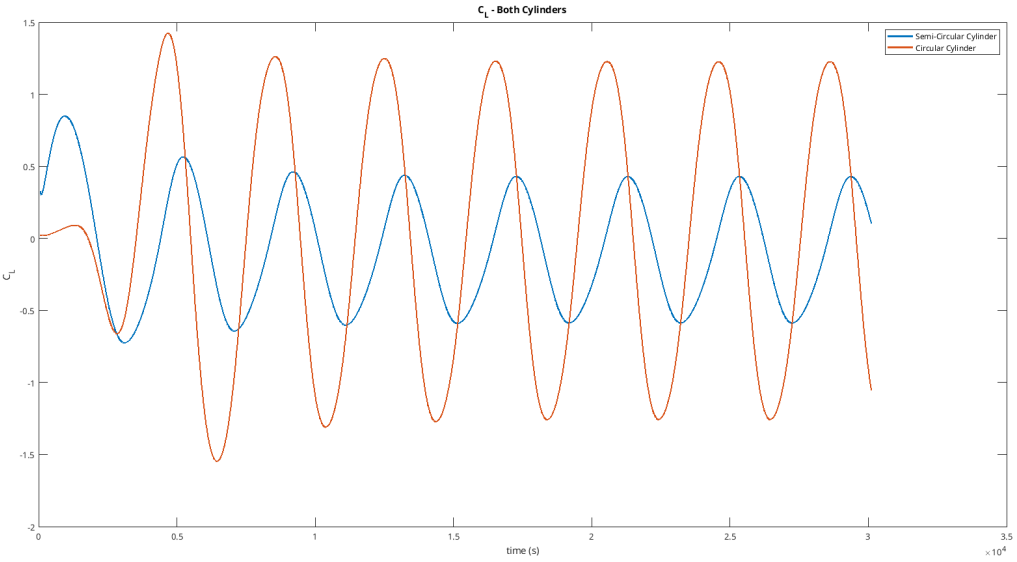


The plot above shows the variation of $C_{L,rms}$ with time for both the cylinders. The lift coefficients vary about a mean at zero and reach a dynamic steady state. The $C_{L,rms}$ is higher for the circular cylinder as a result of incident flow on the circular cylinder is highly inclined in the vertical direction due to the shear layers shed by the semicircular cylinder. The inclination of the semicircular cylinder hampers lift generation due creation of high pressure regions at the top flat surface.

## 4.2 Nusselt Number

The mathematical formulations of the local and average Nusselt number $(Nu)$ are given by

$$Nu_l = -\frac{\frac{\partial T}{\partial \boldsymbol{n}}}{T_w - T_\infty}$$

where $\boldsymbol{n}$ is the direction normal to the surface. The average $Nu$ can be then calculated as

$$Nu_{avg} = \frac{1}{l}\int_l Nu_l dl$$

The Nusselt numbers for different time steps are calculated by evaluating the wall heat fluxs, which are essentially the Temperature gradient flux and then averaged over time. The deviations in Nusselt number for the semicircular cylinder and circular cylinder are $\sim 6\%$ and $\sim 2\%$ respectively. Thus, the heat transfer has been modeled reasonably well by the numerical model.

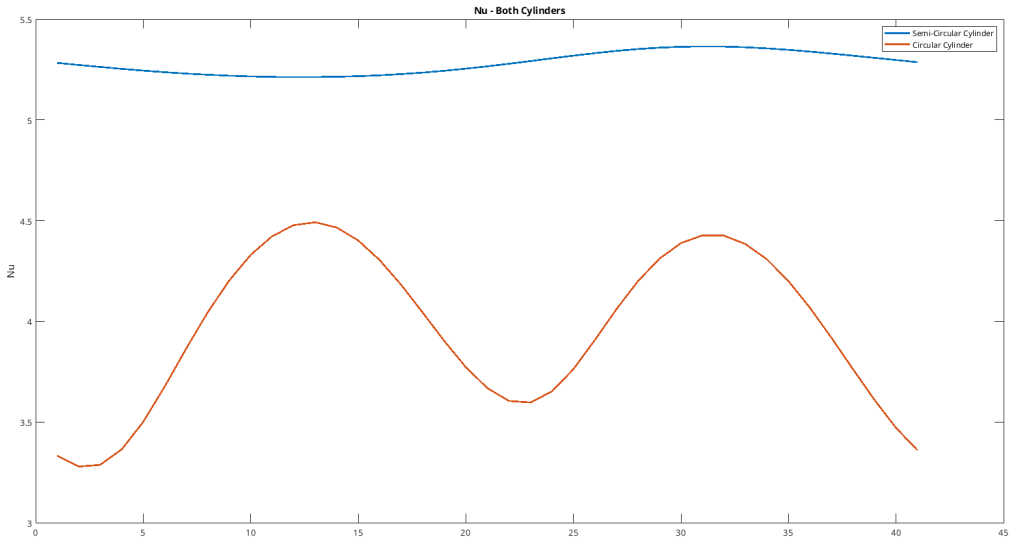


The above plot shows the variation of Nusselt number over a single period of oscillation of the semicircular cylinder. The $Nu$ is higher for the semicircular cylinder as a consequence of it being in incidence with the freestream.

## 4.3 Strouhal Number

The unsteady forced convection over this arrangement of bluff bodies exhibits Von Karman Vortex Shedding. The frequency of the periodic Vortex Shedding in its dimensionless form is Strouhal number of the flow. It is expressed as

$$St = \frac{fD}{u_\infty}$$

where $f$ is the frequency, $D$ is the characteristic length and $u_\infty$ is the freestream velocity.
The Strouhal number was calculated by performing *Fast Fourier Transform (FFT)* of the time data of Drag Coefficient $C_{D,rms}$ over the circular cylinder.

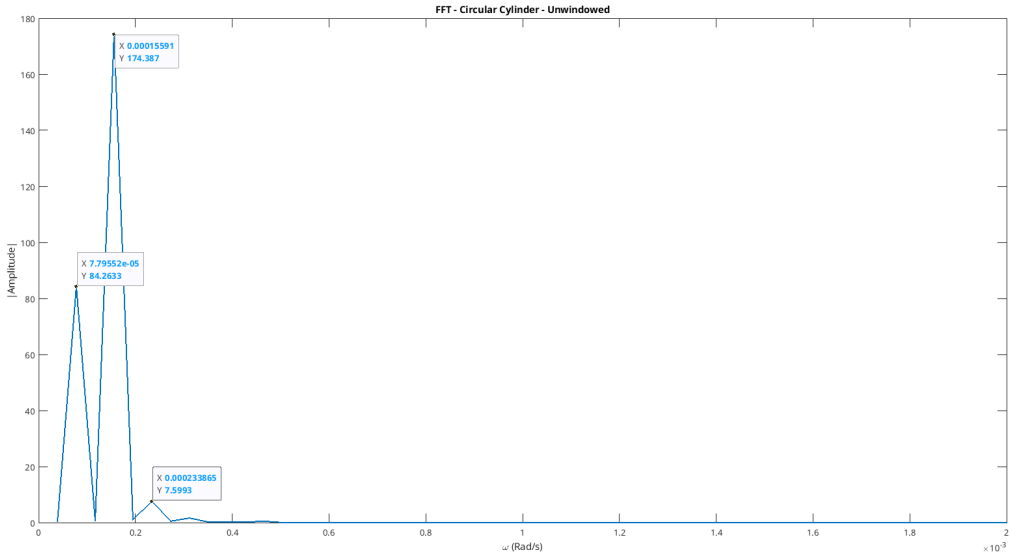


The frequency distribution of the signal obtained by FFT is shown above. The peak harmonic frequency is chosen for Strouhal number calculation. There is a significant difference in the results in literature and current numerical model (deviation $\sim$ 33%). The authors [1] have calculated the Strouhal number by sampling velocity signal at a distance $5D$ downstream from the circular cylinder, however, in the current study, the drag coefficient signal $C_{D,rms}$ of the circular cylinder is used. This difference, along with numerical modeling deficiencies contribute to the error in Strouhal number.

## 4.4 Contours and Streamlines

The streamlines along with temperature, vorticity and pressure contours have been presented in this section. Resemblance with the plots in the reference [1] have been observed. All the contours are plotted at a specific time instant.

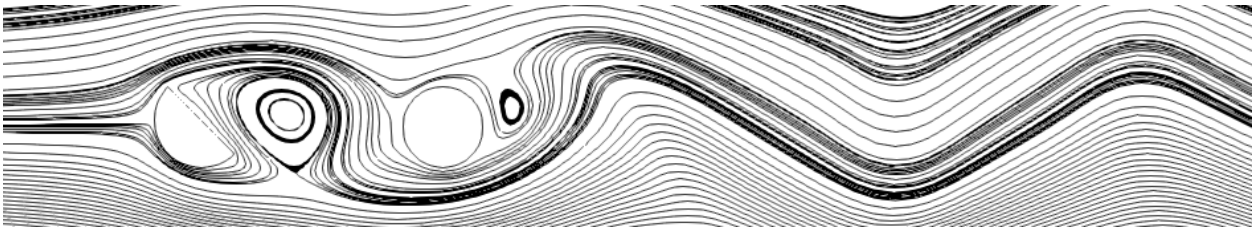

The plot above depicts the streamlines over the cylinder. Two re-circulation zones at this time instant can be observed behind the cylinders. The larger re-circulation zone is observed in the wake region behind the semicircular cylinder.

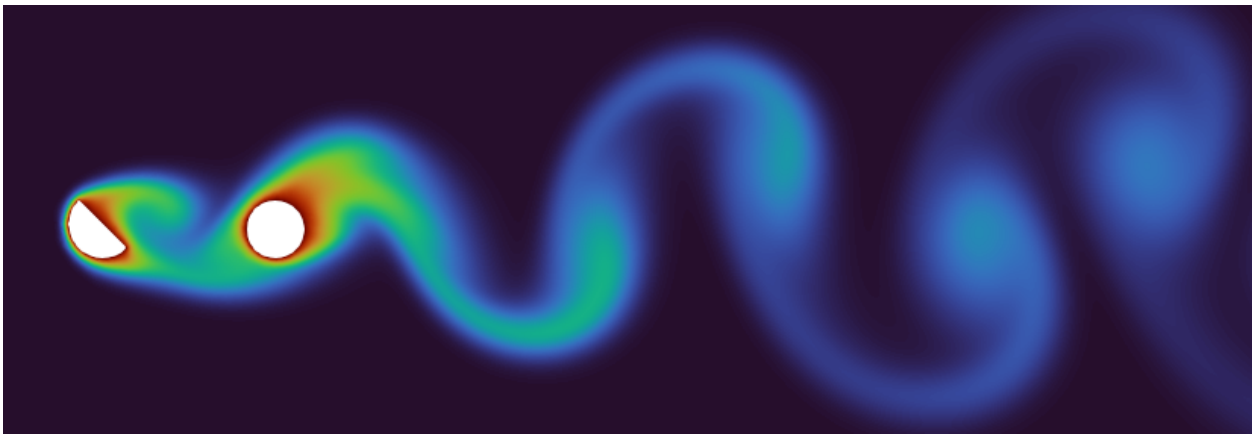

Temperature contours can be seen in the contour plot above. The thermal transport takes place with the formation of boundary layers, and hence is transported with the separating shear layers and the vortices. Hot vortex blobs with decreasing temperatures can be observed due to heat transfer with surrounding cold fluid outside the vortices.

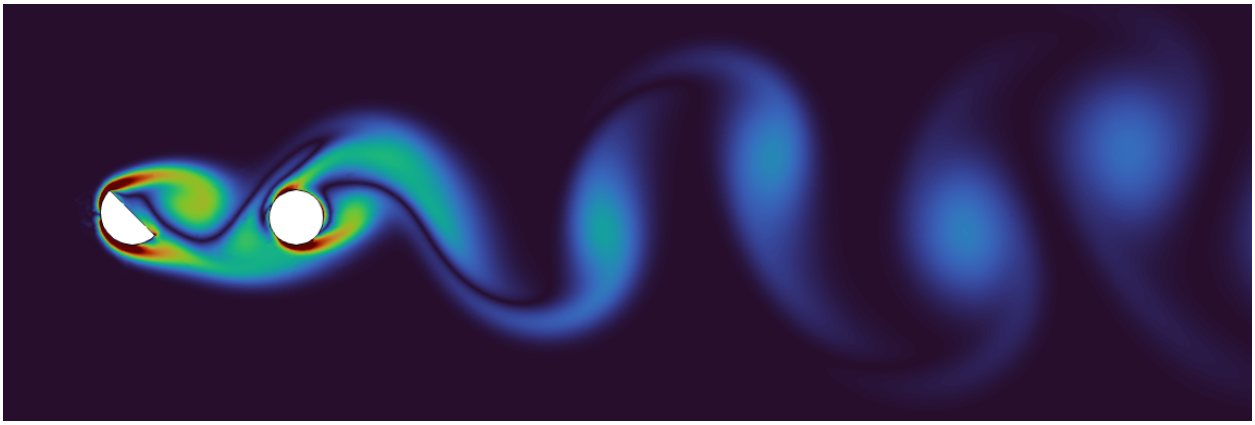

The plot above shows the vorticity contours. High vorticity is observed at incidence of semi-circular cylinder and in the direction of incoming flow for the circular cylinder. The vortices shed alternatively have opposite vorticities, however the plot above displays only the vorticity magnitude.

The pressure contours can be seen in the contour plot above. We can observe a high pressure region at the stagnation at incidence of semicircular cylinder. Further, the high velocity regions and the vortices shed are regions of low pressure. Significantly low pressures are observed in the large re-circulation zone between the cylinder.

# References

[1] Sarkar, S., Mondal, C., Manna, N. K., and Saha, S. K. (2021). Forced convection past a semi-circular cylinder at incidence with a downstream circular cylinder: Thermofluidic transport and stability analysis. *Physics of Fluids*, 33(2):023603.

DISCLAIMER: This project reproduces the results from an existing work, which has been acknowledged in the report. Any query related to the original work should not be directed to the contributor of this project.